

Screening and fluctuation of topological charge in random wave fields

L. DE ANGELIS¹ AND L. KUIPERS^{1,*}

¹Kavli Institute of Nanoscience, Delft University of Technology, 2600 GA, Delft, The Netherlands

*Corresponding author: l.kuipers@tudelft.nl

Compiled July 4, 2018

Vortices, phase singularities and topological defects of any kind often reflect information that is crucial to understand physical systems in which such entities arise. With near-field experiments supported by numerical calculations, we determine the fluctuations of the topological charge for phase singularities in isotropic random waves, as a function of the size R of the observation window. We demonstrate that for 2D fields such fluctuations increase with a super-linear scaling law, consistent with a $R \log R$ behavior. Additionally, we show that such scaling remains valid in presence of anisotropy. © 2018 Optical Society of America

OCIS codes: (260.6042) Singular optics; (180.4243) Near-field microscopy; (140.1540) Chaos.

<http://dx.doi.org/10.1364/ao.XX.XXXXXX>

An accurate knowledge on the statistical fluctuations of a given physical observable is often essential, with an importance on par with the ensemble-averaged value of the observable itself [1]. In fact, fluctuations are ubiquitous in quantum as well as in classical physics. A prime example is the grand canonical ensemble in statistical physics, where the number of particles is only known in average, and its fluctuations have an actual physical meaning, directly linked to the chemical potential of the system [2]. Ensembles of this type are offered by many systems in physics, for example whenever they exhibit topological defects [3, 4], which in the context of optics can be optical singularities [5]. These singularities are point-like entities carrying a topological charge and in random waves they are reminiscent of interacting particles [6]. Oppositely charged pairs can be created and destroyed [7], resulting in a total number of singularities which is not conserved. Although the total topological charge of an ensemble of singularities is always conserved [8], this number can still vary when considering a finite observation window, and its fluctuations are the hallmark for intrinsic properties of the system, such as charge screening [9].

Here we study quantitatively the fluctuations of the

total topological charge for phase singularities in random waves and determine the dependence of such fluctuations on the size of the observation window. With near-field experiments we map the optical near-field inside a chaotic cavity [6]. By tuning the excitation wavelength we measure different realizations of the optical random wave pattern inside the cavity [10]. Such phase- and polarization-resolved measurements enable us to pinpoint position and topological charge of the individual phase singularities in all in-plane components of the electric field that we measure, and therefore determine and investigate their total topological charge and its fluctuations. With experimental evidence, corroborated by numerical calculations, we demonstrate that the sum of the topological charges contained in a square region of area R^2 fluctuates as $R \log R$, in agreement with analytical calculations [9].

We generate optical random waves by coupling infrared monochromatic light into a chaotic cavity [Fig. 1(a)]. This consists of a 220 nm silicon membrane on a silica buffer, patterned with a photonic crystal which encloses the cavity area. The shape of this area was engineered so to ensure random wave propagation in the cavity [11, 12]. By means of near-field optical microscopy we map amplitude, phase and polarization of the in-plane optical field inside the cavity [13]. While our measurements provide access to the two-dimensional random vector field, previous theoretical results describe the behavior of a scalar quantity [9]. With this regard, it is important to note that our complete information on the in-plane field \mathbf{E} allows us to reconstruct an out-of-plane component $H_z \propto \mathbf{k} \times \mathbf{E}$, which behaves fully as a scalar field [6]. Following well established models for random wave fields [12], we can think of H_z as an isotropic superposition of plane waves interfering with random phases $\phi_{\mathbf{k}}$ [14],

$$H_z = \sum_{|\mathbf{k}|=k_0} \exp(i\mathbf{k} \cdot \mathbf{r} + i\phi_{\mathbf{k}}), \quad (1)$$

which is characterized by an autocorrelation

$$C(r) = \int d\mathbf{r}' H_z(\mathbf{r}') H_z(\mathbf{r} + \mathbf{r}') = J_0(kr), \quad (2)$$

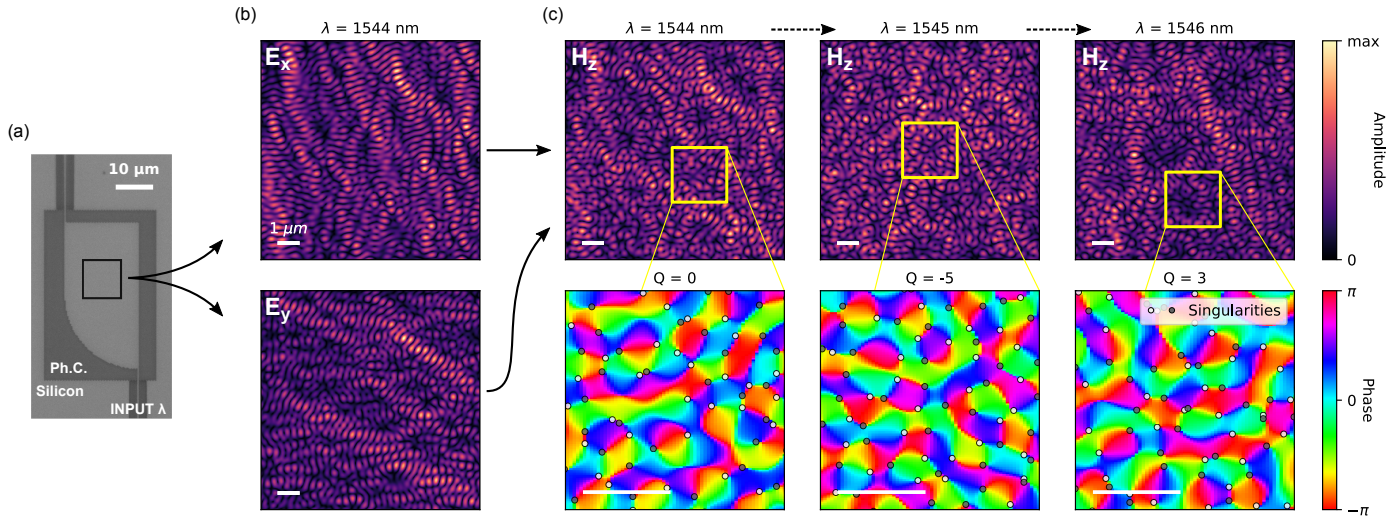


Fig. 1. Overview of the near-field measurements of the optical field inside the chaotic cavity. (a) Optical micrograph of the cavity used for the generation of the optical random wave field. The dark area is the photonic crystal that confines light inside the cavity. (b) Example of a direct measurement of the in-plane components of the optical random field under investigation. In the upper panel the amplitude of E_x and in the lower pane the amplitude of E_y . (c) Near-field maps of $H_z \propto \mathbf{k} \times \mathbf{E}$. In the upper panels the amplitude of H_z for different excitation wavelength λ , and in the lower panels zoomed-in images of its phase. Phase singularities of positive and negative topological charge are depicted by light-gray and dark-gray circles, respectively.

where $J_0(kr)$ is the Bessel function of order 0.

Figure 1 presents a direct measurement of the amplitude of the in-plane field components (E_x, E_y), as well as amplitude and phase of H_z , as obtained from measurements at different excitation wavelength. From the sub-wavelength maps of the amplitude we can clearly resolve the interference that results in a speckle-like pattern [15]. Figure 1 also displays zoomed-in images for the phase of H_z . Here, the circles indicate the location of phase singularities with their topological charge (color), i.e., the integer number of times that the phase of the field loops from $-\pi$ to π around the singular point. We pinpoint the location of each singularity by integrating the phase variations at the experimental limit of two by two pixels, which sets our spatial resolution to be at best equal to the pixel size, of approximately 20 nm. We always observe the topological charge to be ± 1 (dark/light gray) [5]. The patterns presented in Fig. 1 change dramatically with the input wavelength. A wavelength shift of 1 nm already leads to a totally different field configuration. In fact, the spectral correlation width of this random field is of the order of 0.2 nm, as we quantify by computing the wavelength-wavelength correlation of H_z [10].

Although the wave field is made up by randomly interfering waves, the distribution of the singularities does contain structure. In fact, the distribution of phase singularities in random waves has a liquid-like correlation [6, 14, 16]. An immediate question that arises at this point, is whether the charges of such distribution of singularities are correlated or not, and, if so, how. In a system of charged particles we would expect such correlation to

occur due to charge screening. While it is tempting to make an analogy straight away, and predict a screening among topological charges, we must remember that the nature of phase singularities is radically different from that of atoms and molecules, and there is no true and measurable physical interaction among these entities. A straightforward analogy between charged particles and singularities with their topological charge is therefore not so trivial.

The easiest test that can be performed to determine the existence of charge screening, is to measure the overall topological charge $Q = \sum_i q_i$ of the singularities q_i contained in an area of dimension $A = R^2$. In complete absence of charge correlation one expects the average $\langle Q \rangle$ of such quantity to be zero, and its variance $\langle Q^2 \rangle$ to scale with the area of the observation window R^2 [9]. A screening among charges would reveal itself by slowing down the dependence of such variance to a sub-quadratic law. In fact, screening neutralizes charges by surrounding them with a cloud of opposite charges, so to prevent fluctuations of the total charge inside an area $\sim R^2$, in favor of fluctuations along the perimeter region $\sim R$ [17]. The existence of screening among topological charges is well established in literature. [9, 17–24]. It starts to play a role when the size of the observation window is bigger than the typical inter-singularity distance, of approximately $\lambda/2$. However, how much this screening slows down the quadratic law $\langle Q^2(R) \rangle \propto R^2$ is yet unclear. Explicitly, a first model of $\langle Q^2(R) \rangle$, in which two assumptions were made on the autocorrelation of the random field, predicted linear scaling [18], whereas further theory de-

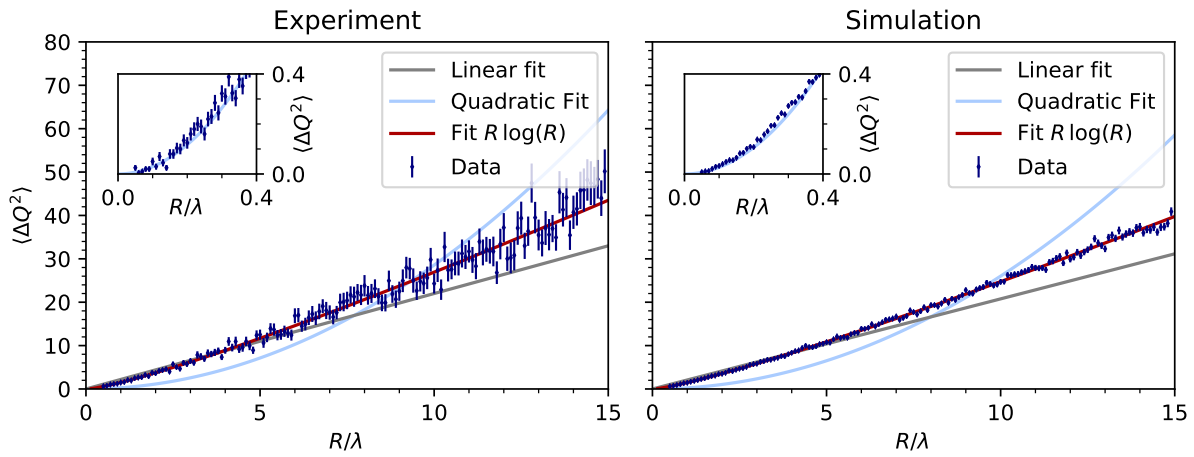


Fig. 2. Fluctuation of topological charge $\langle \Delta Q^2 \rangle$ as a function of the size R of the observation area R^2 , for the experimental scalar field H_z (a) and for a simulated isotropic scalar field (b). The blue errorbars are the respective data points. The gray lines are the best fit with $f_1 = mR$ [$m_{exp} = 2.20(5)$; $m_{sim} = 2.08(4)$]. The red lines are the best fit with $f_2 = a b R \log b R$ [$a_{exp} = 0.026(5)$, $b_{exp} = 19(3)$; $a_{sim} = 0.0144(1)$, $b_{sim} = 30(2)$]. The light blue lines are the best fit with $f_3 = cR^2$ [$c_{exp} = 0.286(11)$; $c_{sim} = 0.260(11)$].

velopments proved such quantity to scale as $R \log R$ [9]. More recently, also paraxial experiments were performed, supporting the linear dependence [17, 22, 23].

Figure 2 presents our results for $\langle Q^2(R) \rangle$. In the main plots the analysis of screening for $R \geq \lambda/2$, in the inset a proof of its absence in the region $R < \lambda/2$. In the left panel we present the experimental data, which is the result of the sampling of 200 experimental scalar field realizations where we randomly pick the position of our observation window. The fields are obtained by varying the excitation wavelength λ over a range $\Delta\lambda = 20$ nm around $\lambda_0 = 1550$ nm. In the right panel we show simulation data, realized by sampling 3500 random wave fields which were independently calculated by adding up 250 plane waves with isotropic directions and random phases [Eq. (2)]. In both cases, we obtain a good agreement only with the $R \log R$ dependence. A quadratic fit cR^2 is clearly inadequate for the data displayed in the main plot. However, this functional behavior perfectly describes the short-distance data in the insets of Fig. 2, at which range screening is indeed absent. Less evident, but still significant, is the inconsistency between the data and a linear behavior. Although this is more eye-catching in the region $R/\lambda > 5$, a clear deviation is still present for $R/\lambda < 3$, with even greater significance considering the small errorbars associated with the latter region.

More quantitatively, we fitted our data with $f_1(R) = mR$ (gray lines in Fig. 2), and $f_2(R) = a b R \log b R$ (red lines in Fig. 2). We focus on how well these functions can describe our data rather than on the resulting fit parameters, which we found to depend on the shape of the chosen observation window (not shown). We quantified the goodness of such least-square fits by performing a χ^2 test, the results of which are summarized in Table 1. In both experiment and simulation we are performing the

fit on 145 equally spaced data points, resulting in 144 degrees of freedom (DOF) for the linear fit (1 free parameter) and in 143 DOF for f_2 (2 free parameters). The χ^2 is a stochastic variable, with expectation value equal to the DOF [25]. The values of the χ^2 for the fittings with $f_2(R)$ are consistent with their expectation value, whereas the case of f_1 leads to χ^2 values that are too high to be mere statistical fluctuations. After this quantitative analysis of our fits we can most certainly conclude that the $R \log R$ scaling law is describing the behavior of $\langle Q^2(R) \rangle$ better than a linear function.

Fit function	χ^2_{exp}	χ^2_{sim}	DOF
$f_1(R) = mR$	954	10^4	144
$f_2(R) = a b R \log b R$	125	147	143

Table 1. Summary of the χ^2 tests for the least-square fits presented in Fig. 2 (isotropic case).

Certainly, the studied cases are not exhaustive of all the possible functional behaviors one could think of. For instance, an alternative trade-off between the linear and quadratic scalings could be given by a generic power law βR^α . Interestingly, such a function can be effectively used to fit both experimental and simulated data, with $\alpha \approx 1.2$. However, the result of such fits (not shown) are found to be less reliable, since they lead to different optimal fit parameters when varying fitting range. In the absence of existing theories, they remain difficult to interpret.

Going back to screening and its nature, we now investigate its role in presence of anisotropy. In fact, in case of anisotropic wave propagation also the spatial arrangement of phase singularities becomes anisotropic [6],

and it does not resemble the distribution of a simple liquid anymore. Actually, along particular directions the resulting distribution is more reminiscent of an ordered structure. Thus, it is interesting to check whether or not this anisotropy influences the topological screening here discussed.

Anisotropic wave propagation naturally takes place in the single vector components of the measured in-plane electric field. This is caused by the strict relation between polarization and propagation direction set by transverse electric propagation [6]. Figure 1(b) presents an example of our direct measurement of amplitude E_x and E_y inside the chaotic cavity. By comparing this figures to the maps for the scalar field H_z presented in Fig. 1(c), we can see a pronounced anisotropy. For example, in the amplitude map of E_x we easily distinguish a stripy pattern, given by a fast modulation of the amplitude along the y -axis, opposed to a modulation along the x -axis which is slower by at least a factor two. This anisotropy results in a spatial arrangement of dislocations where many singularities with the same topological charge are displaced along the y -axis, while the first neighbor in the x -direction is often oppositely charged [6].

Figure 3 presents the fluctuation of topological charge $\langle \Delta Q^2 \rangle$ for the case of E_x , in both experiment and simulation. The analysis of its behavior is carried in complete analogy to what already described for H_z . Again, we can conclude that the scaling law given by $R \log R$ is more successful than a linear function [$\chi_{exp}^2(mR) = 2098$ vs $\chi_{exp}^2(a b R \log b R) = 187$]. However, we do observe that the growth rate of $\langle \Delta Q^2 \rangle$ is faster than in the case of the scalar field H_z (Fig. 2). This suggests that an anisotropic distribution of topological charges results in a screening that on average is less effective with respect to its isotropic counterpart. This of course only holds when considering the average over all the possible directions along which singularities are displaced, whereas it is very likely for this form of screening to strongly depend on the considered direction. Still, considering these qualitative differences

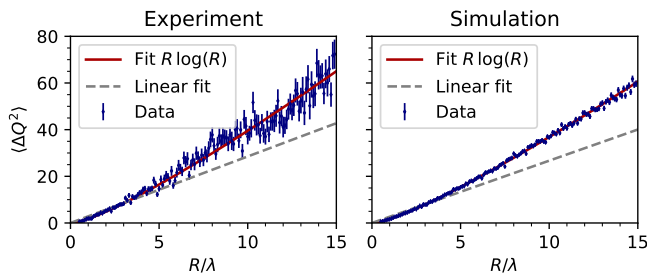


Fig. 3. Fluctuation of the topological charge $\langle \Delta Q^2 \rangle$ vs. R , as in Fig. 2. These results are for the anisotropic case of a Cartesian component (E_x) of a transverse vector field \mathbf{E} . Gray lines $f_1 = mR$ [$m_{exp} = 2.85(9)$; $m_{sim} = 2.08(4)$]. Red lines $f_2 = a b R \log b R$ [$a_{exp} = 0.15(2)$, $b_{exp} = 6.5(5)$; $a_{sim} = 0.126(3)$, $b_{sim} = 6.9(1)$].

with the isotropic scalar case, it is remarkable how the $R \log R$ law can still describe the data.

To conclude, we presented a quantitative study on the screening of topological charges for singularities in random waves. With near-field experiments and numerical calculations we demonstrated that while the average topological charge remains zero independently of the size R of the observation window, the fluctuation of this quantity increases with a dependence which is consistent with a $R \log R$ law. This result validates previous analytical theory [9]. Additionally, we extended our study to the case of anisotropic wave propagation, and even though the nature of screening drastically changes, we showed that the functional dependence of topological charge fluctuations is still well described by the $R \log R$ scaling law.

We thank Andrea Di Falco for fabricating the chaotic cavity used in the near-field experiments, Su-Hyun Gong for critical reading of the manuscript and Filippo Alpeggiani for useful discussions. This work is part of the research program of the Netherlands Organization for Scientific Research (NWO). The authors acknowledge funding from the European Research Council (ERC Advanced Grant No. 340438-CONSTANS).

REFERENCES

1. S. Balibar, *Nature* **451**, 136 (2008).
2. D. Frenkel and B. Smit, *Understanding molecular simulation: from algorithms to applications*, vol. 1 (Academic press, 2001).
3. M. M. Genkin, A. Sokolov, O. D. Lavrentovich, and I. S. Aranson, *Phys. Rev. X* **7**, 011029 (2017).
4. S. Prokhorenko, Y. Nahas, and L. Bellaïche, *Phys. Rev. Lett.* **118**, 147601 (2017).
5. J. F. Nye and M. V. Berry, *Proc. R. Soc. Lond. A* **336**, 165 (1974).
6. L. De Angelis, F. Alpeggiani, A. Di Falco, and L. Kuipers, *Phys. Rev. Lett.* **117**, 093901 (2016).
7. X. Cheng, Y. Lockerman, and A. Z. Genack, *Opt. Lett.* **39**, 3348 (2014).
8. G. Gbur, *Optica* **3**, 222 (2016).
9. B. A. van Tiggelen, D. Anache, and A. Ghysels, *Europhys. Lett.* **74**, 999 (2006).
10. L. De Angelis, F. Alpeggiani, A. Di Falco, and L. Kuipers, *Phys. Rev. Lett.* **119**, 203903 (2017).
11. C. Liu, R. E. C. van der Wel, N. Rotenberg, L. Kuipers, T. F. Krauss, A. Di Falco, and A. Fratalocchi, *Nat. Phys.* **11**, 358 (2015).
12. H.-J. Stöckmann, *Quantum chaos: an introduction* (Cambridge university press, Cambridge, 2006).
13. N. Rotenberg and L. Kuipers, *Nat. Photonics* **8**, 919 (2014).
14. M. V. Berry and M. R. Dennis, *Proc. R. Soc. Lond. A* **456**, 2059 (2000).
15. H. Yilmaz, E. G. van Putten, J. Bertolotti, A. Lagendijk, W. L. Vos, and A. P. Mosk, *Optica* **2**, 424 (2015).
16. R. Höhmann, U. Kuhl, H.-J. Stöckmann, J. D. Urbina, and M. R. Dennis, *Phys. Rev. E* **79**, 016203 (2009).
17. R. I. Egorov, M. S. Soskin, D. A. Kessler, and I. Freund, *Phys. Rev. Lett.* **100**, 103901 (2008).
18. I. Freund and M. Wilkinson, *J. Opt. Soc. Am. A* **15**, 2892 (1998).
19. M. R. Dennis, *J. Phys. A-Math. Gen.* **36**, 6611 (2003).
20. D. A. Kessler and I. Freund, *J. Opt. Soc. Am. A* **25**, 2932 (2008).
21. I. Freund and D. A. Kessler, *Opt. Commun.* **281**, 5954 (2008).
22. I. Freund, D. A. Kessler, V. Vasylyev, and M. S. Soskin, *Opt. Lett.* **40**, 4747 (2015).
23. I. Freund, R. I. Egorov, and M. S. Soskin, *Opt. Lett.* **32**, 2182 (2007).
24. A. J. H. Houston, M. Gradhand, and M. R. Dennis, *J. Phys. A-Math. Theor.* **50**, 205101 (2017).
25. W. G. Cochran, *Ann. Math. Stat.* **23**, 315 (1952).